Continuous flashing suppression of neural responses and population orientation coding in macaque V1

[1]Cai-Xia Chen[1#], Xin Wang[1#], Dan-Qing Jiang[1], Shi-Ming Tang[2,3*], & Cong Yu[4*] Mar. 03, 2026

[1] School of Psychological and Cognitive Sciences, [2] School of Life Sciences, and [3] IDG-McGovern Institute for Brain Research, Peking University, Beijing, China, 100871; [4] Department of Psychology and Behavioral Sciences, Zhejiang University, Hangzhou, China

Equal-contribution first authors

* Correspondence authors: Shi-Ming Tang (tangshm@pku.edu.cn) & Cong Yu (yu_cong@zju.edu.cn)

Abstract

Continuous flash suppression (CFS), a dynamic masker presented to one eye suppressing the conscious perception of a stimulus shown to the other eye, has been extensively used to study visual consciousness. Various studies reported high-level visual and cognitive functions under CFS, which, however, has more recently been questioned and at least partially attributed to low-level stimulus properties. A key but unsettled issue is the extent to which the responses of V1 neurons, where inputs from two eyes first merge, are affected, as severely suppressed V1 responses would not sustain high-level processing. Here, we used two-photon calcium imaging to record the responses of large samples of V1 neurons to a grating stimulus under CFS in awake, fixating macaques. The results revealed that CFS substantially suppressed V1 orientation responses. Ocularity-wise, it nearly completely eliminated the orientation responses of V1 neurons preferring the masker eye or both eyes, while also significantly suppressing the responses of those preferring the grating eye. Modeling analyses suggest that, under CFS, the brain retains the ability of classifying coarse

orientations, but may become less capable of reconstructing the grating stimulus. Consequently, while CFS-suppressed orientation information still supports low-level orientation discrimination, it may not suffice for high-level visual and cognitive processing.

Introduction

When a target stimulus is presented to one eye and a flickering Mondrian-like masker to the other eye, the target can be rendered invisible for an extended period (Tsuchiya & Koch, 2005). This paradigm, known as continuous flash suppression (CFS), has been widely used to investigate subconscious visual processing (Yang, Brascamp, Kang, & Blake, 2014; Moors, Hesselmann, Wagemans, & van Ee, 2017; Pournaghdali & Schwartz, 2020). Among the most intriguing findings are the subconscious high-level visual and cognitive functions under the influence of CFS (e.g., Fang & He, 2005; Almeida, Mahon, Nakayama, & Caramazza, 2008; Adams, Gray, Garner, & Graf, 2010; Mudrik, Breska, Lamy, & Deouell, 2011; Sklar et al., 2012; Zabelina et al., 2013; Tettamanti, Conca, Falini, & Perani, 2017). For example, as reported, priming effects are evident when the target and the invisible primer are categorically (Almeida et al., 2008) or semantically (Zabelina et al., 2013) consistent. However, many of these observations have been questioned by more recent studies, with at least some of the high-level effects being attributed to low-level feature processing (Guido Hesselmann & Malach, 2011; Sakuraba, Sakai, Yamanaka, Yokosawa, & Hirayama, 2012; Gray, Adams, Hedger, Newton, & Garner, 2013; Moors, Boelens, van Overwalle, & Wagemans, 2016; Moors et al., 2017; Moors & Hesselmann, 2018; Pournaghdali & Schwartz, 2020; Stuit, Paffen, & Van der Stigchel, 2023).

A critical issue in this debate is the impact of CFS on V1 neuronal activity. CFS has been

hypothesized to arise from mechanisms similar to those in binocular rivalry (Tsuchiya & Koch, 2005; Yang et al., 2014; Moors et al., 2017), which likely suppress V1 responses through interocular inhibition. Only the surviving stimulus information would then be relayed to downstream areas for potential subconscious higher-level visual and cognitive processing (Jiang, Costello, & He, 2007; Adams et al., 2010; Almeida, Mahon, & Caramazza, 2010). Importantly, if V1 activity is suppressed to a sufficient degree, the low-level stimulus information carried by the remaining V1 responses may not suffice to sustain high-level processing of more complex stimuli defined by those low-level features.

Two prominent fMRI studies have examined the impact of CFS on V1 activity (Watanabe et al., 2011; Yuval-Greenberg & Heeger, 2013). Watanabe et al. (2011) compared monocular CFS masking (stimulus visible) and dichoptic CFS masking (stimulus invisible), and reported that V1 BOLD responses were largely insensitive to stimulus visibility when attention was carefully controlled. However, using similar experimental design, Yuval-Greenberg and Heeger (2013) observed reduced BOLD responses in V1 under dichoptic masking, suggesting that V1 activity changed with stimulus visibility. They attributed the difference of results between two studies mainly to differences in number of trials and thus the statistical power (~250 trials per condition vs. ~90 trials per condition). Nevertheless, these studies contrasted monocular and dichoptic masking conditions to equate stimulus input while manipulating perceptual visibility, which were not designed to quantify the pure effect of CFS on stimulus-evoked V1 responses, that is, the difference of BOLD signals between binocular masking and stimulus alone conditions. In contrast, original psychophysical studies (Tsuchiya & Koch, 2005; Tsuchiya, Koch, Gilroy, & Blake, 2006) demonstrated CFS masking by contrasting the visibility of the target stimulus with and without the presence of dichoptic mask. Consequently, the impact of CFS on V1 activity should be larger than what has been reported by Yuval-Greenberg

and Heeger (2013).

Neurons in V1 exhibit various degrees of ocular dominance (Hubel & Wiesel, 1962), which influences each neuron's binocular combination of monocular visual inputs from two eyes (Kato, Bishop, & Orban, 1981; Mitchell, Carlson, Westerberg, Cox, & Maier, 2023; Zhang, Zhao, Jiang, Tang, & Yu, 2024). In the present study, we used a with-or-without-dichoptic-masker design similar to those used in original psychophysical studies, and examined the extent to which V1 neuronal responses were affected by CFS and how neurons preferring the target eye, masker eye, or both eyes were differently impacted. Using a customized two-photon imaging setup for awake macaques (Li, Liu, Jiang, Lee, & Tang, 2017), we sampled large neural populations at cellular resolution and measured ocular dominance for each individual neuron. This approach enabled us to investigate the potentially differential impacts of CFS on the responses of V1 neurons with varying ocular preferences, as well as apply machine learning tools to understand the impacts of CFS on V1 orientation coding at the population level.

Results

We used two-photon calcium imaging to record responses of V1 superficial neurons from two awake, fixating macaques, each with two response fields of view (FOVs, 850 x 850 μm^2) (Fig. 1A). During the initial recording, the stimulus was a binocular 0.45-contrast square-wave grating varying at twelve orientations and two spatial frequencies (3 & 6 cpd) (Fig. 1B). A total of 3,564 neurons were identified through image processing, including 3,004 (84.29%) orientation-tuned neurons that were included in following data analyses.

The same grating stimulus was then presented monocularly (Fig. 1B) to each eye to characterize individual neurons' eye preferences. Each neuron's ocular dominance index (ODI)

was calculated as ODI = $(R_i - R_c)/(R_i + R_c)$, where R_i and R_c were the neuron's peak responses to ipsilateral and contralateral stimulations, respectively. Neurons with an ODI at –1 or +1 would exclusively prefer the contralateral or ipsilateral eye, while neurons with an ODI at 0 would prefer both eyes equally. Consistent with previous findings (Hubel & Wiesel, 1962; Horton & Hocking, 1996; Livingstone, 1996; Zhang et al., 2024), neurons with similar eye preferences clustered together (Fig. 1C), indicating ocular dominance columns. The ODI followed unimodal distributions (Fig. 1D), in which the majority of neurons were binocular, showing comparable preferences for either eye. Only a small portion of neurons were monocular, being more responsive to the ipsilateral or contralateral eye.

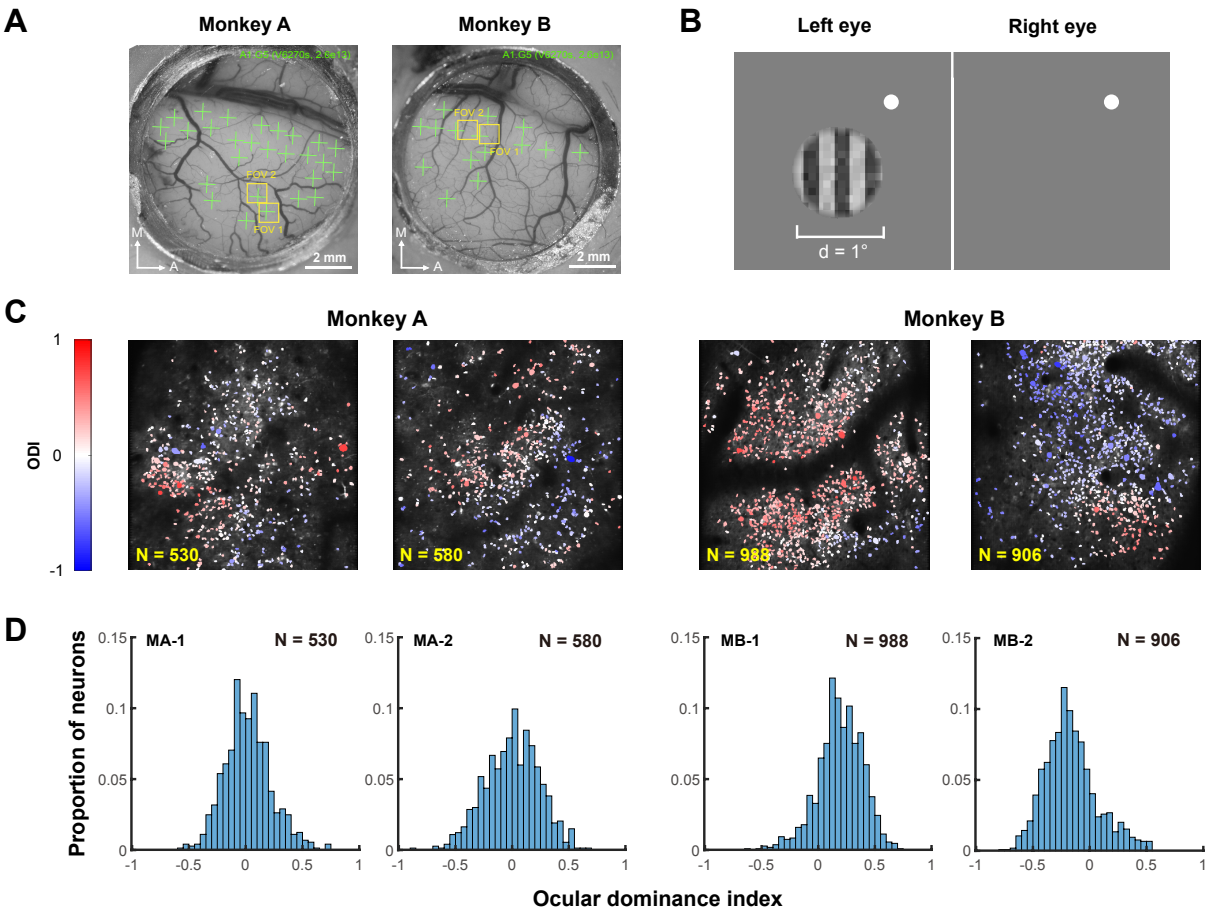

Figure 1. Two-photon imaging and ocular dominance mapping. **A**. Optical windows for imaging of two macaques. Green crosses indicate the regions for viral vector injections, and yellow boxes

107 indicate the FOVs chosen for imaging. **B**. Stimuli used for OD mapping. A circular-windowed
108 square-wave grating was presented monocularly to each eye, respectively, to probe each neuron's
109 ODI. **C**. Ocular dominance functional maps of each FOV at single-neuron resolution showing OD
110 clusters. **D**. Frequency distributions of individual neurons' ODIs in each FOV.

111 In a third and last step, the grating stimulus and the flashing noise masker were
112 presented dichoptically to evaluate the impact of CFS on neurons' orientation responses (Fig.
113 2A). The results are summarized as population orientation tuning functions under the baseline
114 no-CFS condition and the CFS condition following the procedure in Busse, Wade, and Carandini
115 (2009). Specifically, neurons with similar orientation preferences were binned (bin width = 15°)
116 relative to the target orientation for a total of 12 bins, and the resultant population orientation
117 tuning functions based on the mean responses of these bins (Fig. 2C) were fitted with a
118 Gaussian function. Compared to the baseline population orientation tuning functions, those
119 under the influence of CFS displayed profound reductions in orientation response. The
120 amplitude decreased by 84.18% in Monkey A and 60.78% in Monkey B on the basis of
121 Gaussian fitting, while the slope decreased by 91.31% in Monkey A and 71.50% in Monkey B
122 (Fig. 2B). These results support the conclusion of Yuval-Greenberg and Heeger (2013) that V1
123 activity is degraded by CFS, 'akin' to a loss in the contrast-to-noise ratio of neural activity.

124 Furthermore, neurons were divided into three groups according to their ODIs, and the
125 impacts of CFS on their respective orientation responses were examined: neurons preferring
126 the grating eye (ODI > 0.2 or < -0.2, depending on whether the grating stimulation was
127 ipsilateral or contralateral), binocular neurons (-0.2 <= ODI <= 0.2), and neurons preferring the
128 masker eye (ODI < -0.2 or > 0.2 relative to the grating eye). Compared to the baseline
129 condition, the orientation tuning of neurons preferring the masker eye was completely wiped
130 out by CFS (Fig. 2B, D left), leading to flattened tuning curves with unmeasurable amplitudes

or bandwidths. The orientation tuning of binocular neurons was either nearly completely wiped out (Monkey A) or substantially abolished (Monkey B) (Fig. 2B, D middle). There were 85.68% and 68.32% decreases in amplitude, and 92.64% and 77.07% decreases in slope, for Monkeys A and B, respectively. The orientation tuning of neurons preferring the grating eye was the least but still substantially affected (Fig. 2B, D right), with respective 77.78% and 41.75% decreases in amplitude and 85.23% and 57.56% decreases in slope for two monkeys.

To quantify the loss of V1 population orientation encoding due to continuous flash suppression (CFS), we compared the Fisher information (Averbeck & Lee, 2006) under both baseline and CFS conditions. Here, Fisher information serves as a statistical measure that reflects how much information the responses of neurons can provide about the grating orientation. Specifically, it indicates the sensitivity of neural responses to small changes in orientation, in that higher values signify greater precision in encoding orientation information. As illustrated in Fig. 2E, Fisher information was reduced by CFS primarily for orientations deviated by less than 15° from the neurons' preferred orientations. The average Fisher information for stimuli within this 15° range decreased to 29.1% and 43.4% of the baseline values in two macaques, respectively (Fig. 2F), indicating the detrimental impact of CFS on the ability of V1 populations to accurately encode and represent orientation information, especially for orientations closely aligned with neuronal preferences.

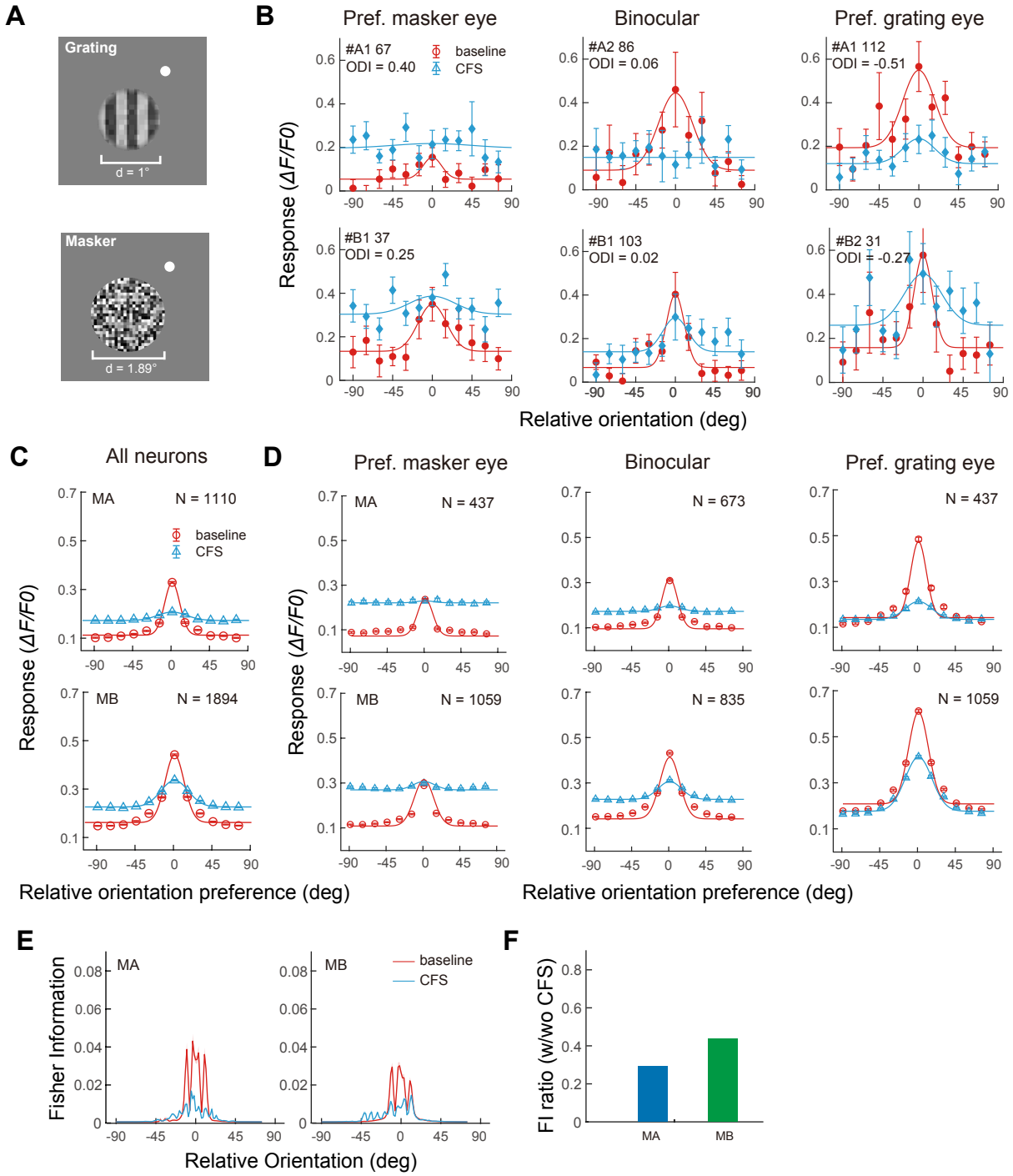

Figure 2. The impacts of CFS on population orientation tuning in two macaques. **A**. Stimuli used in the CFS experiment for one macaque. The grating target was presented to one eye, which was dichoptically masked by a circular flashing masker presented to the other eye. The white dot was the fixation point. **B**. Exemplar baseline and CFS orientation tuning functions for neurons with different eye preferences based on Gaussian fitting. **C**. Population orientation tuning functions of all neurons without CFS as the baseline and with CFS based on Gaussian fitting. Data from two FOVs

of each monkey were pooled due to highly consistent results. **D**. Population orientation tuning functions of sub-groups of neurons with different eye preferences without and with CFS. Data from two FOVs of each monkey were pooled. Curves are fitting results using an ocular dominance-dependent gain control model. Error bars represent ±1 SE. **E**. The impacts of CFS on Fisher information. Fisher information is plotted as a function of relative orientation (to the neuron's preferred orientation) without and with CFS. Shaded areas denote ±1 SE. **F**. The ratio of baseline/CFS Fisher information within 15° of neurons' preferred orientations. Data from two FOVs of each monkey were pooled due to highly consistent results.

An ocular-dominance-dependent gain control model

We developed an ocular dominance-dependent gain control model to account for the impact of CFS on V1 population orientation tuning. The model development followed two steps.

Step I. Population orientation tuning functions before CFS

The population orientation tuning functions due to monocular stimulation exhibited different amplitudes among OD groups (Fig. 2D, red curves), which could be simulated with Equation 1, an OD-weighted Gaussian basis function:

$$\boldsymbol{R} = \boldsymbol{w}^{s} \times \left[A \times \ exp^{-\left(\frac{\theta}{\sigma}\right)^{2}} + B \right] \qquad \text{(Eq. 1)}$$

where parameters A, σ, and B corresponded to the amplitude, standard deviation, and minimal response of the Gaussian basis function, respectively, and θ represented the preferred orientation of a bin of neurons relative to the actual orientation of the grating stimulus. The weight parameter w was the mean of linearly transformed ODIs of neurons in a neuronal group, which equated to *(ODI +1)/2* or *1 - (ODI + 1)/2*, depending on contralateral or

ipsilateral eye grating stimulation, and ranged from 0-1. Thus, a smaller *w* would indicate a higher preference for the eye seeing the grating, and a larger *w* would indicate a higher preference for the unstimulated eye (or the eye seeing the flashing masker under CFS). The *w* equated to 0.33, 0.50, and 0.67 in Monkey A, and 0.32, 0.5, and 0.68 in Monkey B, for the grating eye-preferring group, binocular group, and the masker eye-preferring group, respectively. The exponent *s* represented a nonlinear transformation.

Equation 1 fitted the baseline data well (Fig. 2D, red curves), resulting in goodness-of-fit (R^2) values at 0.94 and 0.95 for the two monkeys, respectively. This indicated that the equation captured the OD-dependent population orientation tuning characteristics of V1 neurons with monocular stimulation before CFS.

Step II. The impacts of CFS

In step II, the model introduced several binocular combination factors to account for population orientation tuning functions under CFS.

To account for the OD-dependent changes of orientation tuning bandwidths under CFS, a *w*-dependent inhibition factor w^t was introduced, which scaled the σ of the tuning functions, changing the monocular tunings R into R':

$$\mathbf{R}' = \boldsymbol{w}^s \times \left[\mathrm{A} \times exp^{-\left(\frac{\theta}{\sigma \times \boldsymbol{w}^t}\right)^2} + \mathrm{B}\right] \qquad \text{(Eq. 2)}$$

This allowed different groups of neurons to exhibit various degrees of orientation tuning function broadening, capturing the pattern in which neurons preferring the eye seeing the grating displayed a sharper population orientation tuning curve under CFS than those preferring the eye seeing the masker.

Previous studies have shown that binocular neuronal responses can be modeled by incorporating interocular suppression and summation processes (Kato et al., 1981; Dougherty, Cox, Westerberg, & Maier, 2019; Zhang et al., 2024). Therefore, R' was further normalized by the neural response to the flashing masker to simulate interocular suppression, which was the first component of Equation 3. Additionally, the neural response to the flashing masker was summed to simulate binocular summation, which was the second component of Equation 3. These two components when summed, determining the final neural responses under CFS:

$$\mathbf{R}_{CFS} = \frac{R'}{aN^k} + bN^m \qquad \text{(Eq. 3)}$$

where *N* was the empirical neural response to the monocularly presented flashing masker stimulation, *a* and *b* were scaling parameters, and *k* and *m* were nonlinearity parameters. The interocular normalization by masker response led to amplitude reduction of population orientation tuning functions for different groups of neurons, while the binocular summation with masker response elevated the minimal responses of tuning functions to their corresponding heights.

During the step II model fitting, the parameters *A*, *σ*, and *s* were inherited from the monocular tuning fits derived from Equation 1 and served as inputs, while the parameters *a*, *k*, *b*, *m*, and *t* were optimized. The model captured the CFS modulation on population orientation tuning curves well, with R^2 = 0.99 and 0.98 for Monkeys A and B, respectively (Fig. 2D, red curves).

Orientation classification and reconstruction under CFS

223 What are the impact of CFS-induced suppression on V1 orientation decoding? To
224 answer this question, which is crucial for understanding subconscious processing under CFS,
225 we trained linear decoders to classify neighboring stimulus orientations (15°) in our
226 experiments, as well as transformer models to reconstruct the stimulus images. Here,
227 orientation classification was parallel to coarse orientation discrimination, and image
228 reconstruction was parallel to orientation recognition, both suggesting the upper bounds of
229 performance assuming an ideal observer.

230 For orientation classification, we trained an all-pair multiclass support vector machine
231 (SVM) classifier to discriminate 12 orientations based on trial-by-trial population neural
232 responses from all trials (Allwein, Schapire, & Singer, 2000). Decoders for different FOVs,
233 ipsilateral/contralateral target presentations, and baseline vs. CFS conditions were trained
234 separately. Under the baseline condition, the decoders achieved mean classification accuracies
235 of 89.5 ± 2.0% and 91.5 ± 2.1% across ipsilateral and contralateral eye conditions in Monkeys A
236 and B, respectively, in contrast to a chance level of 8.3% (1 out of 12). Under CFS, decoding
237 accuracy slightly decreased in Monkey A (81.7 ± 1.9%) but remained stable in Monkey B (90.4
238 ± 2.1%, Fig. 3A). These results suggest that under CFS, there is still sufficient information for
239 coarse orientation discrimination, even for Monkey A whose V1 neuronal responses were
240 substantially suppressed.

241 Next, we trained transformer models to reconstruct the grating images on the basis of
242 corresponding neuronal responses under baseline and CFS conditions. The motivation for this
243 part of the modeling work was the assumption that high-level tasks would be difficult to carry
244 out if the basic stimulus features forming more complex patterns were not intact. Our
245 transformer model contained an architecture that integrated embedding, self-attention, and

246 unembedding modules, as well as a fully connected feedforward layer (Fig. 3B). The model
247 inputs were the responses of all neurons within a FOV to the grating stimulus (ipsilateral and
248 contralateral presentations of the same stimulus were modeled separately), and the model
249 output was the reconstructed grating image. During the training process, the model typically
250 reached two successive learning plateaus, where the validation loss temporarily stagnated
251 (Fig. 3C). Moreover, the validation loss decreased more rapidly when training on the baseline
252 neural response data compared to the CFS data. To compare the differences, we identified the
253 epoch at which the validation loss of the baseline model reached 75% of its total decrease
254 between the two plateaus using a sigmoid fit, and then we retrained both the baseline and
255 CFS models up to this epoch.

256 The retained baseline models reconstructed the grating stimuli significantly better than
257 the CFS models in Monkey A, but this discrepancy was less pronounced in Monkey B (Fig. 3D),
258 consistent with the neuronal data that Monkey A exhibited substantially more CFS suppression
259 than Monkey B in terms of population orientation tuning and Fisher information (Fig. 2). We
260 used a structural similarity index (SSIM) (Brunet, Vrscay, & Wang, 2012) to quantify the
261 reconstruction performances. Across the grating-presenting ipsilateral and contralateral eyes,
262 the baseline models reconstructed the grating with median SSIMs of 0.52 and 0.61 for the two
263 FOVs of Monkey A, and 0.57 and 0.63 for the two FOVs of Monkey B, respectively, while the
264 corresponding SSIMs for the CFS models were 0.16 and 0.19 for Monkey A, and 0.55 and 0.53
265 for Monkey B (Fig. 3E).

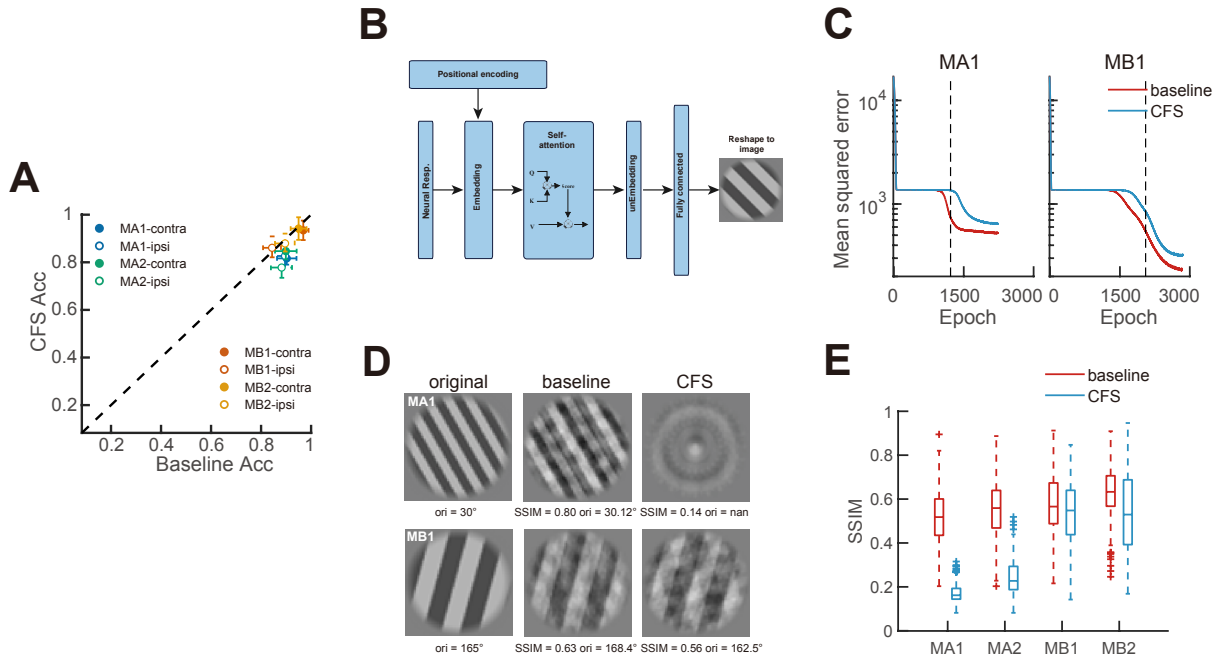

Figure 3. Decoding consequences of CFS revealed by machine learning. **A**. Multiway orientation classification accuracies under CFS vs. baseline conditions obtained using SVM decoders. Each datum represents results from a contralateral or ipsilateral grating condition with a specific FOV averaged across 10-fold cross-validations. Error bars denote 95% confidence intervals. **B**. A diagram of the transformer model for stimulus image reconstruction. **C**. Exemplar learning curves of transformer models under baseline and CFS conditions from two FOVs. The vertical dashed line indicates the epoch at which the baseline model reaches 75% of its total loss decrease between the two learning plateaus estimated using a sigmoid fit. **D**. Illustrations of corresponding reconstructed stimulus images on the basis of learning curves in C. **E**. Box plots of SSIM scores between the original and reconstructed images with baseline and CFS transformers. Within a FOV, results from contralateral eye and ipsilateral eye conditions are combined.

To estimate the impact of CFS-induced V1 suppression on downstream processing, we also recorded neuronal responses from two V2 FOVs in Monkey A (FOVs 3 & 4). As anticipated, V2 neurons were binocular, with over 90% of them showing ODIs within the range of -0.2 to 0.2 (Fig. 4A). Similar to V1 results from the same monkey, CFS on average reduced the

amplitudes of the population orientation tuning functions by 80.05% and the slopes by 89.44% (Fig. 4B). It also reduced the Fisher information to 33.1% of the baseline value (Fig. 4C). Furthermore, we applied the same orientation classification and image reconstruction procedures to the V2 data. For orientation classification, the SVM decoders achieved near-perfect performance in classifying 12 orientations under both baseline and CFS conditions, with classification accuracies exceeding 94% across all cases (Fig. 4D). In the image reconstruction task, the baseline model outperformed the CFS model. Specifically, the baseline transformer models reconstructed the stimulus images with the median SSIM values of 0.61 and 0.53 for the two V2 FOVs, respectively, which dropped to 0.42 and 0.18 in the CFS models (Fig. 4E), implying poorer or failed reconstruction of stimulus images.

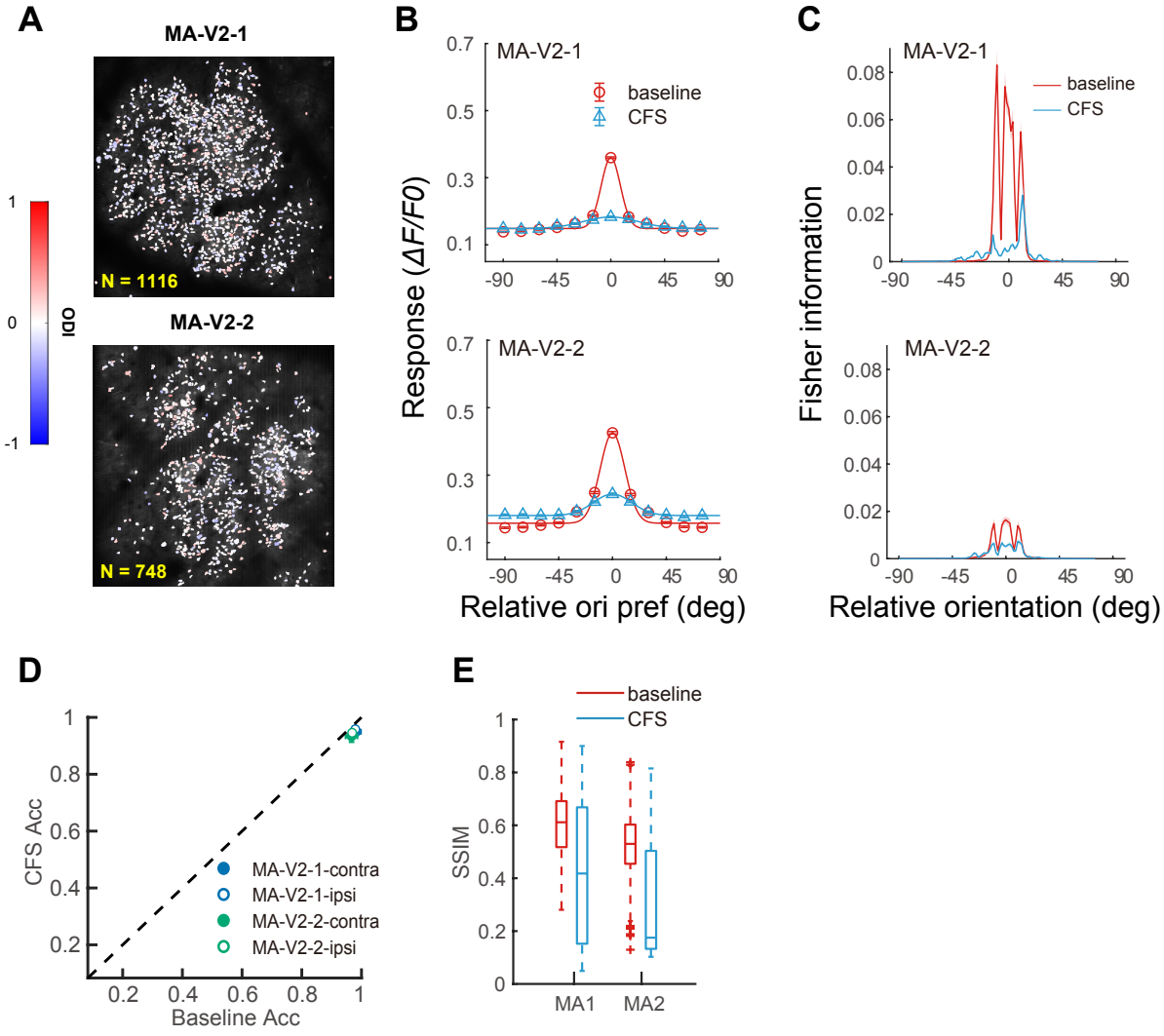

Figure 4. Effects of CFS on V2 orientation responses. **A**. OD maps of the two V2 FOVs of Monkey A (MA3 & MA4). **B**. Population orientation tuning functions for all orientation-tuned neurons with baseline and CFS conditions. Curves represent the results of Gaussian fittings. Error bars represent ±1 SE**. C**. Fisher information as a function of the relative orientation (to the neuron's preferred orientation) with baseline and CFS conditions. Shaded areas denote ±1 SE. Fisher information was lower in MA4 due to higher variations in the data. **D**. Multiway orientation classification accuracies under CFS vs. baseline conditions using SVM decoders. Each datum represents results from a contralateral or ipsilateral grating condition with one FOV, averaged across 5-fold cross-validations. Error bars denote 95% confidence intervals. **E**. Box plots of SSIM scores between the original and reconstructed images with baseline and CFS transformers. Within a FOV, results from contralateral eye and ipsilateral eye conditions are combined.

Discussion

Our study demonstrates that CFS severely compromises orientation information in V1 neurons in an ocular dominance-dependent manner. Orientation information carried by neurons preferring the masker eye or both eyes is completely or nearly completely wiped out, while information carried by those preferring the grating eye is partially retained. Downstream, orientation information in V2 neurons is also substantially weakened. Linear decoding and transformer models suggest that CFS-compromised orientation information may still allow coarse orientation discrimination, but will most likely impair orientation recognition when the suppression is sufficiently strong as in Monkey A. Similarly strong suppression is also possible in Monkey B if the current grating contrast (0.45) is lower to be 0.1-0.3 as in many CFS experiments (Watanabe et al., 2011; Yuval-Greenberg & Heeger, 2013; Lunghi & Pooresmaeili, 2023; Alais, Coorey, Blake, & Davidson, 2024).

CFS-compromised V1 orientation information transmits for downstream visual processing, which may explain the unconscious orientation processing observed in human CFS studies. The “invisible” orientation information can be processed, as demonstrated by adaptation (Kanai, Tsuchiya, & Verstraten, 2006; Bahrami, Carmel, Walsh, Rees, & Lavie, 2008) and priming (Koivisto & Grassini, 2018) studies. The adaptation aftereffect is reduced compared to the visible condition but not entirely abolished (Kanai et al., 2006; Bahrami et al., 2008), likely a result of the degraded orientation information surviving CFS. For the same reason, the priming effect also decreases during trials in which the stimulus is rendered invisible by CFS, compared to those in which the stimulus is visible or partially visible (Koivisto & Grassini, 2018), as the degraded stimulus information provides insufficient evidence for decision-making, resulting in a diminished priming effect (Dehaene, 2011; Gomez, Perea, & Ratcliff, 2013).

Furthermore, our linear decoding and transformer results can help elucidate the debate on whether visual processing still functions at the categorization level under the influence of CFS. Previous studies have provided evidence for the preserved category information of the target, as demonstrated by tool-specific priming effects (Almeida et al., 2008; Almeida et al., 2010) and differential BOLD response patterns between tools and other object categories under CFS (Guido Hesselmann, Hebart, & Malach, 2011; Tettamanti et al., 2017). However, an intriguing question is: Do these results rather reflect low-level feature differences between tools and other object categories? It has been reported that elongated objects, irrespective of their categorical affiliation, elicit similar priming effects (Sakuraba et al., 2012). Consistent with this, when tools are categorized by their shape (elongated vs. non-elongated), only the neural response patterns elicited by elongated tools can be discriminated from other object categories under CFS (Fogelson, Kohler, Miller, Granger, & Tse, 2014; Ludwig, Kathmann, Sterzer, & Hesselmann, 2015). In line with this interpretation, Guido Hesselmann, Darcy, Rothkirch, and Sterzer (2018) reported that tool-specific priming under CFS does not reliably emerge under conditions designed to produce strong interocular suppression, suggesting that previously observed category effects may reflect access to low-level shape features rather than preserved category representations. Moreover, a recent study measuring the contrast thresholds required to both break from and suppress CFS found that stimuli exhibited similar suppression strengths across various categories (Alais et al., 2024). According to our results, when suppression is too strong to allow for stimulus reconstruction, as in the case of Monkey A (Fig. 3C), the orientation information under CFS may not accumulate to a level sufficient for resolving semantic category boundaries. The latter might require somewhat intact stimulus information, even if subconsciously. However, it could potentially assist in category discrimination when categorical differences lie in certain low-level shape dimensions

354 like orientation, as coarse orientation discrimination appears unaffected by CFS suppression
355 (Fig. 3A).
356 A related issue is the dorsal-ventral CFS hypothesis, which proposes that CFS
357 suppression may disproportionately affect ventral visual processing while relatively preserving
358 dorsal pathways involved in visuomotor functions, potentially allowing category- or action-
359 related information to remain accessible under suppression (Fang & He, 2005). However,
360 subsequent fMRI studies have failed to provide consistent support for this dissociation,
361 reporting either stream-invariant awareness effects (Guido Hesselmann & Malach, 2011;
362 Ludwig et al., 2015; Tettamanti et al., 2017), residual signal in ventral rather than dorsal
363 regions (Guido Hesselmann et al., 2011; Fogelson et al., 2014), or residual low-level feature
364 information/partial visibility rather than preserved dorsal processing (Ludwig et al., 2015).
365 Although our study does not directly test dorsal-ventral dissociations, our V1 results provide a
366 constraint on what information downstream visual pathways could access under suppression.
367 When CFS- induced interocular suppression was strong enough and stimuli reconstruction was
368 markedly reduced, as in the case of Monkey A, the information required for category-level or
369 action-related processing may not be sufficient for high-level cortical representation.
370 Interocular suppression under CFS is known to vary substantially across individuals
371 (Yamashiro et al., 2013; Gayet & Stein, 2017; Blake, Goodman, Tomarken, & Kim, 2019). This
372 inter-individual variability may contribute to the heterogeneity observed in the CFS literature.
373 We also found that the strength of V1 response suppression during CFS differed between two
374 monkeys, as reflected by population orientation tuning functions (Fig. 2C), Fisher information
375 (Fig. 2F), and reconstruction performance by the transformer (Fig. 3E). Several experimental
376 factors may have contributed to the relatively weaker suppression observed in Monkey B.
377 Because monkeys viewed the stimuli passively, we could not determine the dominant eye for

each monkey (instead we switched the eyes and averaged the results), and the target was presented at relatively high contrast. Both factors are known to reduce the effectiveness of CFS suppression (Yang, Blake, & McDonald, 2010; Yuval-Greenberg & Heeger, 2013). In addition, the random-noise masker we used might not be as effective as Mondrian patterns (G. Hesselmann, Darcy, Ludwig, & Sterzer, 2016). If reduced stimulus contrast and a Mondrian masker were used, we predict that CFS suppression in Monkey B would strengthen, potentially approaching the level observed in Monkey A. Nevertheless, it is worth emphasizing that our main conclusions are primarily based on data from Monkey A, who exhibited much stronger CFS suppression.

Materials and Methods

Monkey preparation

Monkey preparation was identical to procedures reported in previous studies (Ju, Guan, Tao, Tang, & Yu, 2020; Guan, Ju, Tao, Tang, & Yu, 2021; Zhang et al., 2024). Two rhesus monkeys (*Macaca mulatta*, aged 5 and 6, respectively) underwent two sequential surgeries under general anesthesia and strictly sterile conditions. During the first surgery, a 20-mm diameter craniotomy was performed on the skull over V1. The dura was opened and multiple tracks of 100-150 nil AAV1.hSynap.GCaMP5G.WPRE.SV40 (AV-1-PV2478, titer 2.37e13 (GC/ml), Penn Vector Core) were pressure-injected at a depth of ~350 µm at multiple locations. The dura was then sutured, the skull cap was re-attached with three titanium lugs and six screws, and the scalp was sutured. After the surgery, the animal was returned to the cage and treated with injectable antibiotics (Ceftriaxone sodium, Youcare Pharmaceutical Group, China) for one week. Postoperative analgesia was also administered. The second surgery was performed 45 days later. A T-shaped steel frame was installed for head stabilization, and an optical window

402 was inserted onto the cortical surface. Data collection could start as early as one week later.
403 More details about the preparation and surgical procedures can be found in Li et al. (2017).
404 The procedures were approved by the Institutional Animal Care and Use Committee, Peking
405 University.
406
407 *Behavioral task*
408 After a ten-day recovery period following the second surgery, monkeys were placed in
409 a primate chair with head restraint. They were trained to hold fixation on a small white spot
410 (0.2°) with eye positions monitored by an Eyelink-1000 eye tracker (SR Research) at a 1000-Hz
411 sampling rate. During the experiment, trials with the eye position deviated 1.5° or more from
412 the fixation before stimulus offset were discarded as ones with saccades and repeated.
413
414 *Visual stimuli and experimental procedures*
415 Visual stimuli were generated with a Matlab-based Psychtoolbox-3 software (Pelli &
416 Zhang, 1991) and presented on a ROG Swift PG278QR monitor (refresh rate = 120 Hz,
417 resolution = 2560 × 1440 pixel, pixel size = 0.23 mm × 0.23 mm). The screen luminance was
418 linearized by an 8-bit look-up table, and the mean luminance was 47 cd/m^2. The viewing
419 distance was 60 cm.
420 A drifting square-wave grating (spatial frequency = 4 cpd, contrast = full, speed = 3
421 cycles/sec, starting phase = 0°, size = 0.4° in diameter) was first used to determine the
422 population receptive field (pRF) location, shape, and approximate size associated with a
423 specific FOV. The same stimulus was also monocularly presented to confirm the V1 location as
424 ocular dominance columns would appear. This fast process used a 4 × objective lens mounted
425 on the two-photon microscope and did not provide cell-specific information. The recorded V1

426 pRFs were centered at ~0.90° eccentricity in Monkey A and ~1.93° in Monkey B. V2 pRFs were
427 centered at ~0.67° in Monkey A. All pRFs were approximately circular with a diameter of 0.9°.
428 The target stimulus used in the experiments was a 0.45-contrast circular-windowed
429 square-wave grating. It drifted at 4 cycles per second in opposite directions perpendicular to
430 the orientation with a starting phase of 0°, and varied at 12 orientations (0° to 165° in 15°
431 increments) and two spatial frequencies (3 & 6 cpd) trial by trial. The circular envelope had a
432 diameter of 1°, which approximated the size of pRFs for recorded FOVs, with the edge blurred
433 by a linear ramp starting at a radius of 0.38°. The flashing masker was a circular white noise
434 pattern with a diameter of 1.89°, a contrast of 0.5, and a flickering rate of 10 Hz. The white
435 noise consisted of randomly generated black and white blocks (0.07° × 0.07° each). The target
436 grating and the flashing masker were presented through a pair of NVIDIA 3D Vision 2 active
437 shutter glasses. To mitigate the ghost image, a low contrast (RMS contrast = 0.08) white noise
438 was added to the grating. The width of the noise element was half of the bar width of the
439 square grating, and the white noise was regenerated every frame.
440 Each block of trials consisted of four groups of stimuli: binocular, monocular, CFS, and
441 flashing masker-only. In the binocular group, the grating was presented to both eyes
442 simultaneously. The relevant data were only used to help identify ROIs and orientation-tuned
443 neurons along with data from other stimulus conditions. In the monocular group, the grating
444 was monocularly presented to the contralateral or ipsilateral eye, which served as the baseline
445 conditions without the influences of CFS. In the CFS group, the grating and flashing masker
446 were presented dichoptically. In the flashing masker-only group, the flashing masker was
447 presented monocularly to either eye. Each stimulus condition was repeated for 10-12 trials.
448 For conditions involving the grating, the trials were split for two opposite drifting directions. A

449 block of trial contained 242 trials, two trials for each stimulus condition, with the order of
450 stimulus conditions arranged in a pseudorandom manner. There were 5 to 6 blocks of trials
451 with each FOV.
452 Each stimulus was presented for 1000 ms, followed by an inter-stimulus interval of
453 1500 ms, allowing sufficient time for the calcium signals to return to the baseline level (Guan,
454 Zhang, Zhang, Tang, & Yu, 2020). For each FOV, the recording was completed in a single
455 session with 5-6 experiment blocks and lasted for 2-3 hours.
456
457 *Two-photon imaging*
458 Two-photon imaging was performed using a FENTOSmart two-photon microscope
459 (Femtonics), along with a Ti:sapphire laser (Mai Tai eHP, Spectra Physics). GCaMP5 was chosen
460 as the indicator of calcium signals because the fluorescence activities it expresses are linearly
461 proportional to neuronal spike activities within a wide range of firing rates from 10-150 Hz (Li
462 et al., 2017). During imaging, a 16× objective lens (0.8 N.A., Nikon) with a resolution of 1.6
463 µm/pixel was used, along with a 1000 nm femtosecond laser. A fast resonant scanning mode
464 (32 fps) was chosen to obtain continuous images of neuronal activity (8 frames per second
465 after averaging every 4 frames). The strength of fluorescent signals (mean luminance of a
466 small area) was monitored and adjusted if necessary for the drift of fluorescent signals. Two
467 response fields of view (FOVs) measuring 850 × 850 μm^2 in V1 were selected in both
468 macaques, and two FOVs of the same size in V2 were selected in Macaque A.
469
470 *Imaging data analysis: Initial screening of ROIs*
471 Data were analyzed with customized MATLAB codes. A normalized cross-correlation
472 based translation algorithm was used to reduce motion artifacts (Li et al., 2017). Then the

473 fluorescence changes were associated with corresponding visual stimuli through the time
474 sequence information recorded by Neural Signal Processor (Cerebus system, Blackrock
475 Microsystem). By subtracting the mean of the 4 frames before stimuli onset (*F0*) from the
476 average of the 6th-9th frames after stimuli onset (*F*) across 5 or 6 repeated trials for the same
477 stimulus condition (same orientation, spatial frequency, size, and drifting direction), the
478 differential image ($\Delta F = F - F0$) was obtained.

479 For a specific FOV, the regions of interest (ROIs) or possible cell bodies were decided
480 through sequential analysis of 242 differential images in the order of CFS, monocular,
481 binocular, and flashing masker-only conditions. CFS conditions consisted of 96 ($2\times2\times12\times2$ =
482 96) differential images, with the grating presented to either eye (2), at two spatial frequencies
483 (2), twelve orientations (12), and two motion directions (2). Monocular conditions were
484 identical to the CFS conditions except that the flashing masker was absent. In the binocular
485 conditions, gratings at two spatial frequencies (2), twelve orientations (12), and two motion
486 directions (2) were binocularly presented, resulting in 48 differential images. The flashing
487 masker-only conditions consisted of the flashing masker presented to either eye, resulting in 2
488 differential images.

489 The first differential image was filtered with a band-pass Gaussian filter (size = 2–10
490 pixels), and connected subsets of pixels (>25 pixels, which would exclude smaller vertical
491 neuropils) with average pixel value >3 standard deviations of the mean brightness were
492 selected as ROIs. Then the areas of these ROIs were set to mean brightness in the next
493 differential image before the bandpass filtering and thresholding were performed. This
494 measure gradually reduced the standard deviations of differential images and facilitated the
495 detection of neurons with relatively low fluorescence responses. If a new ROI and an existing
496 ROI from the previous differential image overlapped, the new ROI would be on its own if the

497 overlapping area OA < 1/4 ROI_{new}, discarded if 1/4 ROI_{new} < OA < 3/4 ROI_{new}, and merged with
498 the existing ROI if OA > 3/4 ROI_{new}. The merges would help smoothen the contours of the final
499 ROIs. This process went on through all differential images twice to select ROIs. Finally, the
500 roundness for each ROI was calculated as:

501 $$Roundness = \frac{\sqrt{4\pi \times A}}{P}$$

502 where A was the ROI's area, and P was the perimeter. Only ROIs with roundness larger than
503 0.9, which would exclude horizontal neuropils, were selected for further analysis.
504

505 *Imaging data analysis: Orientation tuning and ocular dominance*

506 The ratio of fluorescence change (*ΔF/F0*) was calculated as a neuron's response to a
507 specific stimulus condition. For a specific neuron's response to a specific stimulus condition,
508 the *F0n* of the n-th trial was the average of 4 frames before stimulus onset (-500 - 0 ms), and
509 *Fn* was the average of the *5th-8th, 6th-9th, or 7th-10th* frames after stimulus onset, whichever
510 was the greatest. *F0n* was then averaged across 10 or 12 repeated trials to obtain the baseline
511 *F0* for all trials (to reduce noise in the calculation of responses), and *ΔFn/F0 = (Fn- F0)/F0* was
512 taken as the neuron's response to this stimulus at the n-th trial.

513 Several steps were taken to determine whether a neuron was orientation-selective. For
514 each monocular or binocular condition, the orientation and SF eliciting the maximal response
515 were designated as the neuron's preferred SF and orientation. We then compared responses
516 across all 12 orientations at the preferred SF by performing a non-parametric Friedman test to
517 determine whether the neuron's responses at various orientations were significantly different
518 from each other. To reduce Type I errors, the significance level was set at $\alpha = 0.01$. Neurons
519 that passed the Friedman test at least under one viewing condition were selected as

orientation-tuned neurons.

The ocular dominance index (ODI) was calculated to characterize each neuron's eye preference: ODI = $(R_i - R_c)/(R_i + R_c)$, where R_i and R_c were the neuron's peak responses at the best orientation and SF to ipsilateral and contralateral monocular grating conditions, respectively. Neurons with an ODI of -1 or 1 would be completely contralateral or ipsilateral eye dominant, and of 0 would be equally dominant by both eyes.

Population orientation tuning

For each neuron, neural responses at the preferred SF were selected for tuning analysis. To derive population orientation tuning curves under a specific condition, we categorized neurons into twelve orientation preference bins according to their preferred orientations (bin width = 15°). For each orientation presented, the responses of all orientation preference bins were reorganized according to the relative orientation preference. Subsequently, neuronal responses of the same relative orientation preference were averaged to generate the final population orientation tuning function. For CFS conditions, the selected SF and binning procedures were the same as their corresponding monocular conditions.

The population orientation tuning function was fitted with a Gaussian model with MATLAB's nonlinear least-squares function 'lsqnonlin':

$$\mathrm{R}(\theta) = \mathrm{a} \times 2^{-\left(\frac{\theta-\theta_0}{\sigma}\right)^2} + b$$

where R(θ) was the response at orientation θ, free parameters a, θ_0, σ, and b were the amplitude, peak orientation, standard deviation of the Gaussian function (equal to half width at half height), and minimal response, respectively.

The population orientation tuning curves for different eye preference groups were

derived using the same procedure, with additional binning of neurons according to their ODI. To obtain the tuning curve of the neurons preferring the eye seeing the grating, responses of neurons with an ODI < -0.2 (preferentially responding to the contralateral eye) under contralateral eye grating presentation and those with an ODI > 0.2 (preferentially responding to the ipsilateral eye) under ipsilateral eye grating presentation were combined. Similarly, for neurons preferring the eye seeing the masker, responses of neurons with an ODI < -0.2 under ipsilateral eye grating presentation and those with an ODI > 0.2 under contralateral eye grating presentation were combined. For binocular neurons (-0.2 < ODI < 0.2), responses under both grating presentation conditions were combined.

Fisher information

The Fisher information assesses the amount of information contained in a neuron population using an optimal decoder (Pouget, Deneve, Ducom, & Latham, 1999). Assume independent Gaussian noise distributions, the Fisher information for a population of N neurons was given as

$$I = \sum_{i=1}^{N} \frac{f_i'(\theta)^2}{\sigma_i(\theta)^2}$$

where $f_i(\theta)$ was the mean activity of neuron i in response to the presentation angle, θ, and $f_i'(\theta)$ was its derivative with respect to θ. We fitted each neuron's response tuning $f_i(\theta)$ and variance tuning $\sigma_i(\theta)$ with Gaussian functions and calculated the averaged Fisher information across neurons at each orientation.

SVM-based orientation classification

In the orientation classification task (Fig. 3A), we trained a support vector machine

(SVM) with a one-vs.-one coding scheme to classify orientations from standardized population neural activity. The SVM decoder was implemented using MATLAB's '*fitcsvm*' function with a linear kernel. To prevent overfitting and evaluate the generalization ability of the model, we employed a 5-fold cross-validation procedure, and the model performance on the validation dataset was reported.

Decoders were trained independently for each experiment condition, resulting in 4 models per FOV (contralateral/ipsilateral × baseline/CFS). Neural response data from two spatial frequencies were used as input, with each neuron treated as a feature. In this way, each model were trained and tested on 288 or 240 samples (2 SFs × 12 orientations × 12/10 repeats).

The transformer model

Model input, output, and training procedure

We implemented a transformer-based model to reconstruct grating stimuli from population neuronal responses recorded under different experiment conditions. The model input was a vector of neuronal responses, each corresponding to an individual neuron, and the output was the reconstructed grating image of size 70 × 70 pixels.

The transfromer was trained independently for each experimental condition, resulting in four models per FOV (contralateral/ipsilateral × baseline/CFS). Pilot experiments revealed that our original dataset was insufficient for the model to converge. To address this, we augmented the dataset to four times its original size before training. Augmentation was performed by sampling from a normal distribution centered at each neuron's response mean, with a standard deviation equal to its original standard deviation. Within the augmented

dataset, 6% was reserved for validation. Responses were normalized to [0, 1] before fed into the model.

We implemented a two-phase training procedure to assess the reconstruction ability of models trained on different neural data. During the training process, the model typically reached two learning plateaus, where the validation loss temporarily stagnated (Fig. 3C). In the first training session, we analyzed the learning curve to determine the epoch at which the baseline model's validation loss had completed 75% of its total decrease between the two plateaus. This was estimated using a modified sigmoid fit:

$$\mathrm{loss(t)} = A - \frac{C}{1 + e^{k(b-t)}}$$

where *A* and *C* defined the function range, *b* was the symmetry point, *k* was the steepness parameter, and *t* represented the epoch number, counted from epoch 500 (initial epochs were discarded due to a drastic drop in validation loss across all training runs, see Fig. 3C). The 75% decrease point was computed as:

$$\text{Stop point} \ = \ \mathrm{b} + \frac{\ln\,(3)}{k}$$

In the second training session, we retrained both models up to the identified epoch and evaluated their performances.

The model was trained to minimize the mean squared error (MSE) between the reconstructed and actual stimuli. Optimization was performed using RMSprop with a learning rate of 0.00005 and a smoothing factor ρ = 0.85.

Model structure

Each neuron's response was embedded into a higher-dimensional space using a learned weight vector as follows:

$$R^1 = W^{emb} \odot R^0$$

where the R^0 (n×1) represented the original response vector from n neurons, and W^{emb} (n× d_{model}) was the embedding weight matrix, with each row corresponding to a neuron-specific weight vector. Here we used d_{model} = 2. The symbol ⊙ denoted row-wise multiplication, such that the ith response r_i^0 was multiplied by both elements in its embedding weight vector w_i^{emb}. The resulting embedding matrix R^1 (n×d_{model}) contained the high-dimensional representations of the neuronal responses.

The enriched embedding matrix was then passed through a self-attention module. In this module, R^1 was first projected into queries (Q), keys (K), and values (V) through independent learnable weight matrices, respectively. Then the attention map was computed as:

$$AttentionMap = SoftMax(\frac{QK^T}{\sqrt{d_k}})$$

where d_k represented the dimensionality of the key vectors, which scaled the dot-product to control the variance of the attention scores.

The output of self-attention was calculated as:

$$R^2 = AttentionMap \times V$$

The output from self-attention was unembedded by projecting each neuron's high-dimensional representation back to one-dimensional. A feedforward layer transformed the unembedded vector into a stimulus vector, which was then reshaped into the final 70 × 70 image.

Model evaluation

The original, non-augmented data was used for analysis, which had been seen during training in both the training and validation sets. We used a structural similarity index (SSIM) (Brunet et al., 2012) to quantify the reconstruction performances.

The SSIM (Brunet et al., 2011) between two images x and y (both 70×70) is defined as:

$$SSIM(x,y) = \frac{(2\mu_x\mu_y + c_1)(2\sigma_{xy} + c_2)}{(\mu_x^2 + \mu_y^2 + c_1)(\sigma_x^2 + \sigma_y^2 + c_2)}$$

where μ_x and μ_y are the mean intensities, σ_x^2 and σ_y^2 are the variances, σ_{xy} is the covariance, and c_1 and c_2 are constants for numerical stability.

Acknowledgments

This study was supported by a Natural Science Foundation of China STI2030-Major Projects grant (2022ZD0204600) to SMT and CY.

Competing interests

None.

References

Adams, W. J., Gray, K. L. H., Garner, M., & Graf, E. W. (2010). High-Level Face Adaptation Without Awareness. *Psychological Science, 21*, 205-210.

Alais, D., Coorey, J., Blake, R., & Davidson, M. J. (2024). A new 'CFS tracking' paradigm reveals uniform suppression depth regardless of target complexity or salience. *eLife, 12*, RP91019.

Allwein, E. L., Schapire, R. E., & Singer, Y. (2000). Reducing multiclass to binary: A unifying approach for margin classifiers. *Journal of machine learning research, 1*, 113-141.

Almeida, J., Mahon, B. Z., & Caramazza, A. (2010). The Role of the Dorsal Visual Processing Stream in Tool Identification. *Psychological Science, 21*, 772-778.

Almeida, J., Mahon, B. Z., Nakayama, K., & Caramazza, A. (2008). Unconscious processing dissociates along categorical lines. *Proceedings of the National Academy of Sciences of the United States of America, 105*, 15214-15218.

Averbeck, B. B., & Lee, D. (2006). Effects of Noise Correlations on Information Encoding and Decoding. *Journal of Neurophysiology, 95*, 3633-3644.

Bahrami, B., Carmel, D., Walsh, V., Rees, G., & Lavie, N. (2008). Unconscious orientation processing depends on perceptual load. *Journal of Vision, 8*, 12-12.

Blake, R., Goodman, R., Tomarken, A., & Kim, H.-W. (2019). Individual differences in continuous flash suppression: Potency and linkages to binocular rivalry dynamics.

Vision Research, 160, 10-23.
Brunet, D., Vrscay, E. R., & Wang, Z. (2012). On the Mathematical Properties of the Structural Similarity Index. *IEEE Transactions on Image Processing, 21*, 1488-1499.
Busse, L., Wade, A. R., & Carandini, M. (2009). Representation of concurrent stimuli by population activity in visual cortex. *Neuron, 64*, 931-942.
Dehaene, S. (2011). Conscious and Nonconscious Processes:Distinct Forms of Evidence Accumulation? In Vincent Rivasseau (Ed.), *Biological Physics: Poincaré Seminar 2009* (pp. 141-168). Basel: Springer Basel.
Dougherty, K., Cox, M. A., Westerberg, J. A., & Maier, A. (2019). Binocular Modulation of Monocular V1 Neurons. *Current Biology, 29*, 381-391.e384.
Fang, F., & He, S. (2005). Cortical responses to invisible objects in the human dorsal and ventral pathways. *Nature Neuroscience, 8*, 1380-1385.
Fogelson, S. V., Kohler, P. J., Miller, K. J., Granger, R., & Tse, P. U. (2014). Unconscious neural processing differs with method used to render stimuli invisible. *5*.
Gayet, S., & Stein, T. (2017). Between-Subject Variability in the Breaking Continuous Flash Suppression Paradigm: Potential Causes, Consequences, and Solutions. *Frontiers in Psychology, Volume 8 - 2017*.
Gomez, P., Perea, M., & Ratcliff, R. (2013). A diffusion model account of masked versus unmasked priming: Are they qualitatively different? *Journal of Experimental Psychology: Human Perception and Performance, 39*, 1731-1740.
Gray, K. L., Adams, W. J., Hedger, N., Newton, K. E., & Garner, M. (2013). Faces and awareness: low-level, not emotional factors determine perceptual dominance. *Emotion, 13*, 537-544.
Guan, S.-C., Ju, N.-S., Tao, L., Tang, S.-M., & Yu, C. (2021). Functional organization of spatial frequency tuning in macaque V1 revealed with two-photon calcium imaging. *Progress in Neurobiology, 205*, 102-120.
Guan, S.-C., Zhang, S.-H., Zhang, Y.-C., Tang, S.-M., & Yu, C. (2020). Plaid detectors in macaque V1 revealed by two-photon calcium imaging. *Current Biology, 30*, 934-940.
Hesselmann, G., Darcy, N., Ludwig, K., & Sterzer, P. (2016). Priming in a shape task but not in a category task under continuous flash suppression. *J Vis, 16*, 17.
Hesselmann, G., Darcy, N., Rothkirch, M., & Sterzer, P. (2018). Investigating masked priming along the “vision-for-perception” and “vision-for-action” dimensions of unconscious processing. *Journal of Experimental Psychology: General, 147*, 1641.
Hesselmann, G., Hebart, M., & Malach, R. (2011). Differential BOLD activity associated with subjective and objective reports during "blindsight" in normal observers. *Journal of Neuroscience, 31*, 12936-12944.
Hesselmann, G., & Malach, R. (2011). The link between fMRI-BOLD activation and perceptual awareness is stream-invariant in the human visual system. *Cerebral Cortex, 21*, 2829-2837.
Horton, J. C., & Hocking, D. R. (1996). Intrinsic Variability of Ocular Dominance Column Periodicity in Normal Macaque Monkeys. *The Journal of Neuroscience, 16*, 7228.
Hubel, D. H., & Wiesel, T. N. (1962). Receptive fields, binocular interaction and functional architecture in the cat's visual cortex. *The Journal of Physiology, 160*, 106-154.
Jiang, Y., Costello, P., & He, S. (2007). Processing of Invisible Stimuli: Advantage of Upright Faces and Recognizable Words in Overcoming Interocular Suppression. *Psychological Science, 18*, 349-355.
Ju, N.-S., Guan, S.-C., Tao, L., Tang, S.-M., & Yu, C. (2020). Orientation Tuning and End-

stopping in Macaque V1 Studied with Two-photon Calcium Imaging. *Cerebral Cortex, 31*, 2085-2097.

Kanai, R., Tsuchiya, N., & Verstraten, F. A. J. (2006). The Scope and Limits of Top-Down Attention in Unconscious Visual Processing. *Current Biology, 16*, 2332-2336.

Kato, H., Bishop, P. O., & Orban, G. A. (1981). Binocular interaction on monocularly discharged lateral geniculate and striate neurons in the cat. *J Neurophysiol, 46*, 932-951.

Koivisto, M., & Grassini, S. (2018). Unconscious response priming during continuous flash suppression. *PLOS ONE, 13*, e0192201.

Li, M., Liu, F., Jiang, H., Lee, T. S., & Tang, S. (2017). Long-term two-photon imaging in awake macaque monkey. *Neuron, 93*, 1049-1057.

Livingstone, M. S. (1996). Ocular dominance columns in New World monkeys. *The Journal of Neuroscience, 16*, 2086.

Ludwig, K., Kathmann, N., Sterzer, P., & Hesselmann, G. (2015). Investigating category- and shape-selective neural processing in ventral and dorsal visual stream under interocular suppression. *Human Brain Mapping, 36*, 137-149.

Lunghi, C., & Pooresmaeili, A. (2023). Learned value modulates the access to visual awareness during continuous flash suppression. *Scientific Reports, 13*, 756.

Mitchell, B. A., Carlson, B. M., Westerberg, J. A., Cox, M. A., & Maier, A. (2023). A role for ocular dominance in binocular integration. *Current Biology, 33*, 3884-3895.e3885.

Moors, P., Boelens, D., van Overwalle, J., & Wagemans, J. (2016). Scene Integration Without Awareness: No Conclusive Evidence for Processing Scene Congruency During Continuous Flash Suppression. *Psychol Sci, 27*, 945-956.

Moors, P., & Hesselmann, G. (2018). A critical reexamination of doing arithmetic nonconsciously. *Psychon Bull Rev, 25*, 472-481.

Moors, P., Hesselmann, G., Wagemans, J., & van Ee, R. (2017). Continuous Flash Suppression: Stimulus Fractionation rather than Integration. *Trends Cogn Sci, 21*, 719-721.

Mudrik, L., Breska, A., Lamy, D., & Deouell, L. Y. (2011). Integration without awareness: expanding the limits of unconscious processing. *Psychol Sci, 22*, 764-770.

Pelli, D. G., & Zhang, L. (1991). Accurate control of contrast on microcomputer displays. *Vision Research, 31*, 1337-1350.

Pouget, A., Deneve, S., Ducom, J.-C., & Latham, P. E. (1999). Narrow Versus Wide Tuning Curves: What's Best for a Population Code? *Neural Computation, 11*, 85-90.

Pournaghdali, A., & Schwartz, B. L. (2020). Continuous flash suppression: Known and unknowns. *Psychonomic Bulletin & Review, 27*, 1071-1103.

Sakuraba, S., Sakai, S., Yamanaka, M., Yokosawa, K., & Hirayama, K. (2012). Does the human dorsal stream really process a category for tools? *Journal of Neuroscience, 32*, 3949-3953.

Sklar, A. Y., Levy, N., Goldstein, A., Mandel, R., Maril, A., & Hassin, R. R. (2012). Reading and doing arithmetic nonconsciously. *Proc Natl Acad Sci U S A, 109*, 19614-19619.

Stuit, S. M., Paffen, C. L. E., & Van der Stigchel, S. (2023). Prioritization of emotional faces is not driven by emotional content. *Sci Rep, 13*, 549.

Tettamanti, M., Conca, F., Falini, A., & Perani, D. (2017). Unaware processing of tools in the neural system for object-directed action representation. *Journal of Neuroscience, 37*, 10712-10724.

Tsuchiya, N., & Koch, C. (2005). Continuous flash suppression reduces negative afterimages. *Nature Neuroscience, 8*, 1096-1101.

Tsuchiya, N., Koch, C., Gilroy, L. A., & Blake, R. (2006). Depth of interocular suppression associated with continuous flash suppression, flash suppression, and binocular rivalry. *Journal of Vision, 6*, 6-6.

Watanabe, M., Cheng, K., Murayama, Y., Ueno, K., Asamizuya, T., Tanaka, K., & Logothetis, N. (2011). Attention But Not Awareness Modulates the BOLD Signal in the Human V1 During Binocular Suppression. *Science, 334*, 829-831.

Yamashiro, H., Yamamoto, H., Mano, H., Umeda, M., Higuchi, T., & Saiki, J. (2013). Activity in early visual areas predicts interindividual differences in binocular rivalry dynamics. *Journal of Neurophysiology, 111*, 1190-1202.

Yang, E., Blake, R., & McDonald, J. E., II. (2010). A New Interocular Suppression Technique for Measuring Sensory Eye Dominance. *Investigative Ophthalmology & Visual Science, 51*, 588-593.

Yang, E., Brascamp, J., Kang, M.-S., & Blake, R. (2014). On the use of continuous flash suppression for the study of visual processing outside of awareness. *Frontiers in Psychology, 5*.

Yuval-Greenberg, S., & Heeger, D. J. (2013). Continuous Flash Suppression Modulates Cortical Activity in Early Visual Cortex. *The Journal of Neuroscience, 33*, 9635.

Zabelina, D. L., Guzman-Martinez, E., Ortega, L., Grabowecky, M., Suzuki, S., & Beeman, M. (2013). Suppressed semantic information accelerates analytic problem solving. *Psychon Bull Rev, 20*, 581-585.

Zhang, S.-H., Zhao, X.-N., Jiang, D.-Q., Tang, S.-M., & Yu, C. (2024). Ocular dominance-dependent binocular combination of monocular neuronal responses in macaque V1. *eLife, 13*, RP92839.